Available online at www.sciencedirect.com
ScienceDirect
Biochimica et Biophysica Acta 1768 (2007) 694–704
Biochimica et Biophysica Acta
BBA
www.elsevier.com/locate/bbamem

The role of lipid II in membrane binding of and pore formation by nisin analyzed by two combined biosensor techniques

Katrin Christ [a,*], Imke Wiedemann [b], Udo Bakowsky [c], Hans-Georg Sahl [b], Gerd Bendas [a]

[a] University of Bonn, Department of Pharmacy, An der Immenburg 4, 53121 Bonn, Germany
[b] University of Bonn, Institute for Medical Microbiology, Immunology and Parasitology (IMMIP)-Pharmaceutical Microbiology Unit, Meckenheimer Allee 168, 53115 Bonn, Germany
[c] Philipps University Marburg, Department of Pharmaceutical Technology, Am Ketzerbach 63, 35032 Marburg, Germany

Received 13 September 2006; received in revised form 25 October 2006; accepted 4 December 2006
Available online 15 December 2006

Abstract

Nisin, a peptide antibiotic, efficiently kills bacteria through a unique mechanism which includes inhibition of cell wall biosynthesis and pore formation in cytoplasmic membranes. Both mechanisms are based on interaction with the cell wall precursor lipid II which is simultaneously used as target and pore constituent. We combined two biosensor techniques to investigate the nisin activity with respect to membrane binding and pore formation in real time. Quartz crystal microbalance (QCM) allows the detection of nisin binding kinetics. The presence of 0.1 mol% lipid II strongly increased nisin binding affinity to DOPC (k_D 2.68×10^{-7} M vs. 1.03×10^{-6} M) by a higher association rate. Differences were less pronounced while using negatively charged DOPG membranes. However, lipid II does not influence the absolute amount of bound nisin. Cyclic voltammetry (CV) data confirmed that in presence of 0.1 mol% lipid II, nanomolar nisin concentrations were sufficient to form pores, while micromolar concentrations were necessary in absence of lipid II. Both techniques suggested unspecific destruction of pure DOPG membranes by micromolar nisin concentrations which were prevented by lipid II. This model membrane stabilization by lipid II was confirmed by atomic force microscopy. Combined CV and QCM are valuable to interpret the role of lipid II in nisin activity.

Keywords: Atomic force microscopy (AFM); Cyclic voltammetry (CV); Quartz crystal microbalance (QCM); Lantibiotic; Lipid II; Nisin; Fluorescence recovery after photobleaching (FRAP)

1. Introduction

The antimicrobial peptide nisin is produced by a number of strains of *Lactococcus lactis* and displays antibacterial activity against a broad range of Gram-positive bacteria [1,2]. It belongs to a group of ribosomally synthesized and posttranslationally modified peptides, the lantibiotics. These are characterized by the occurrence of intramolecular rings, formed by the thioether amino acids lanthionine and 3-methyllanthionine [3,4]. Nisin is the most prominent member of the type-A lantibiotics which are elongated, screw-shaped peptides with a net positive charge. These peptides can adopt an amphiphilic structure which has been assumed to be the basis for the bacterial killing mechanism by disturbing the integrity of the energy-transducing bacterial membranes [5]. Besides lantibiotics, other amphiphatic antimicrobial peptides (AMPs), such as pardaxin, alamethicin, oxyopinin, aurein, and magainin have been observed to mediate a membrane disruption. Their mode of action and orientation in membranes was shown to strongly depend on the membrane composition and surrounding [6–10].

However, discrepancies between the micromolar nisin concentrations needed for the disruption of model membranes and the minimal inhibitory concentrations (MIC) in the nanomolar range observed in vivo argue against a simple membrane poration mechanism of nisin. In fact, its activity in nanomolar concentrations was then shown to result from its ability to use the cell wall precursor lipid II as a docking molecule for subsequent pore formation. Apart from pore formation, the binding of lipid II by nisin additionally blocks the cell wall biosynthesis [11], i.e. nisin disposes two killing mechanisms combined in one molecule.

* Corresponding author. Fax: +49228737929.
E-mail address: kchrist@uni-bonn.de (K. Christ).

0005-2736/$ - see front matter © 2006 Elsevier B.V. All rights reserved.
doi:10.1016/j.bbamem.2006.12.003

We recently focused on the time range of pore formation and pore stability by using a black lipid membrane approach [12]. The nisin-induced pores in presence of lipid II have a lifetime in the range of a second and a calculated diameter of about 2 to 2.5 nm. Further experiments using fluorescently labelled lipid II demonstrated that lipid II is not only a target for nisin, but also a constituent of the pore complex recruited by nisin [13]. These studies demonstrated that the pores are of uniform structure and constant nisin/lipid II stoichiometry [14]. More recently, NMR studies have provided further insights into the nisin/lipid II interactions on the molecular level. According to Hsu et al. [15], the N-terminus of nisin forms a cage-like structure that allows the formation of five intermolecular hydrogen bonds between the backbone amides of nisin and the pyrophosphate linkage group of lipid II.

In this work we used a novel combination of two biosensor techniques in a planar model membrane system in order to investigate both, simultaneously, the lantibiotic membrane binding and the pore formation process in real time.

Biosensors are indicated as devices to detect biological recognition processes by transmitting the biological signals into physical measurable effects [16,17]. The quartz crystal microbalance (QCM) is the most prominent method that uses a mass-sensitive transducer. This technique is based on the piezoelectric properties of quartz crystals which enable an electrical excitation and oscillation measurement of a thin quartz plate. The resonance frequency of these oscillations correlates with the mass load on its surface [18]. The QCM method has been established for several analytical approaches, such as characterization of polymer surfaces [19,20] or biological films [21], and ligand–receptor interactions [22–24]. Changes in mass can be detected in real time by monitoring the frequency shifts which additionally allow calculations of the kinetic binding constants k_{ass} (association rate constant), k_{diss} (dissociation rate constant), and k_D (kinetic equilibrium constant). Furthermore, the so called damping analysis allows the evaluation of viscoelastic properties of the surface attached structures. Voluminous structures show high damping effects while tightly bound or small molecules oscillate closely to the quartz.

For the analysis of membrane permeability, cyclic voltammetry is an ideal completion to QCM. CV is based on a triangular potential sweep of the working electrode. The potential is linearly increased from a starting potential to the reversing point, and then decreased with the same rate until the starting potential is reached again. Redox active substances react at the electrode surface by generating a Faradaic current proportional to the reaction rate when their redox potential is reached. Covering the electrodes with model membranes inhibits the transport of the redox active substances to the surface. Consequently, changes in membrane permeability for the redox substances, such as by pore formation, can be monitored by analyzing the peak current. CV experiments have already been applied to investigate film forming [25] or membrane disturbing processes [26].

Considering the potentials and restrictions of both, QCM and CV, it appears promising to apply these techniques for the first time to investigate the lantibiotic activities. QCM allows the detection of lantibiotic binding on membranes while CV can simultaneously detect changes in the membrane barrier function. The use of planar model membranes enables a correlation with microscopic techniques.

In this study we were able to analyze the processes of nisin binding and simultaneous membrane permeabilization separately. The exact calculation of nisin binding kinetics allows an isolated evaluation of binding factors, especially the role of lipid II. Additionally, both devices are able for long term evaluation of nisin interactions with the membrane after pore formation. Further on, this view allows distinguishing the targeted activity from the non-targeted effects of nisin in absence of lipid II. These findings were supported by fluorescence and atomic force microscopy.

2. Materials and methods

2.1. Chemicals

1-Hexadecanethiol ($C_{16}H_{33}SH$), potassium chloride (KCl), hydrogen peroxide (H_2O_2), sulfuric acid (H_2SO_4), potassium ferricyanide ($K_3[Fe(CN)_6]$), and monochlorodimethyloctadecyl-silane ($C_{20}H_{43}SiCl$) were purchased from FLUKA (Neu-Ulm, Germany). The phospholipids 1,2-dioleoyl-*sn*-glycero-3-phosphocholine (DOPC) and 1,2-dioleoyl-*sn*-glycero-3-phosphoglycerol (DOPG), as well as insulin (oxidized B-chain), were obtained from Sigma-Aldrich (Munich, Germany). 1,2-Dioleoyl-*sn*-glycero-3-phosphoethanolamine-*N*-(7-nitro-2-1,3-benzoxadiazol-4-yl) (NBD-PE, Ammonium Salt) was purchased from Avanti Polar Lipids, Inc. (Alabaster, AL, USA). Sodium sulfate (Na_2SO_4), ammonium solution (NH_3), and chloroform ($CHCl_3$) were obtained from Riedel-de Häen (Seelze, Germany).

2.2. Purification of nisin and lipid II

Nisin was purified from culture supernatants of *L. lactis* NIZO22186 [27] by chloroform extraction as described by Bonelli et al. [28]. Nisin was permethylated by reductive methylation of the N-terminus and the lysine residues [29] as performed by Bonev [30]. Complete methylation of nisin, i.e. the incorporation of eight additional methyl groups, was confirmed by mass spectroscopy. The lipid-bound cell wall precursor lipid II was synthesized using membrane preparations of *M. luteus* DSM 1790 and purified as described [31]. The purity of nisin and methylated nisin was 99% (calculated from mass analysis data) and ≥80% for insulin (detected by HPLC). Lipid II was of 98% purity.

2.3. Modification of the quartz crystals and glass slides

The quartz crystals were cleaned as previously described [32] and then put into a chloroform solution of 10 mM $C_{16}H_{33}SH$ for about 12 h to form a self assembled monolayer. The crystals were rinsed with ethanol and dried under air stream conditions.

Microscope glass slides (diameter of 18 mm, thickness of 0.2 mm) were incubated in a H_2O_2/H_2SO_4-mixture (1:3) under ultrasonic conditions for 15 min, completed by rinsing with demineralized water for 10 times. Subsequently, the slides were cleaned with $H_2O_2/NH_3/H_2O$ (1:1:5) under ultrasonic conditions for 15 min. After rinsing again with demineralized water for 15 times the slides were dried at 70 °C. Finally, the slides were incubated with monochlorodimethyloctadecyl-silane at 70 °C for 10 min to create a hydrophobic monolayer. Binding reaction was followed by rinsing with chloroform, washing with water, and drying under air stream conditions.

The immobilization of a second monolayer to complete the supported bilayer was performed by using the Langmuir–Blodgett technique. Therefore lipid monolayers of DOPC ±0.1 mol% lipid II and DOPG ±0.1 mol% lipid II, respectively, were preformed on the air–water interphase of the Langmuir trough. For fluorescence microscope experiments, films contained 1 mol%

NBD-PE. After condensing the lipid layer at a lateral pressure of 38 mN/m, quartz crystals or glass slides were vertically driven through the layer resulting in a complete bilayer. The transfer ratios were between 0.95 and 1. The freshly prepared bilayers were immediately used for the experiments. The quartz crystals were incorporated into the flow chamber under exclusion of air contact to guarantee the integrity of the bilayers.

2.4. QCM measurements

QCM measurements were performed with a LiquiLab21 quartz crystal microbalance (ifak e.V., Barleben, Germany) which enables the simultaneous detection of frequency and damping changes in real time. Measurement chambers were made of polycarbonate with a cell volume of 100 µl. AT-cut quartz crystals with a 10 MHz resonance frequency (14 mm diameter) were supplied by ifak e.V. and modified as described. They were inserted into the measurement chamber to connect the Au-electrodes on both sides of the crystal with the AC voltage supply. The experiments were performed under a volume flow rate (pure water) of 270 µl min^{-1} which roughly corresponds to a shear rate of 5 s^{-1}. After equilibrating the quartz crystals under flow conditions to reach a constant frequency, the indicated concentrations of peptides were added (see Section 2.5). Frequency and damping changes were monitored in real time using specific software. Frequency and damping curves allow for calculation of kinetic binding constants, assuming a first order kinetic of nisin/lipid II interaction. The association rate (k_{ass}) was calculated from the frequency drop according to Eq. 1a, where Δf is the measured frequency change, [A] is the concentration of the injected peptide, and f_{max} is the maximum frequency change for the complete loaded quartz crystal.

$$\Delta f = -\frac{k_{ass}*[A] + f_{max}}{k_{ass}*[A] + k_{diss}} * \left(1 - e^{\{-k_{ass}*[A]+k_{diss}*(t-t_0)\}}\right) \quad (1a)$$

Rinsing with pure water leads to a small frequency increase which allows the calculation of the dissociation rate constant (k_{diss}), according to Eq. 1b, where f_0 is the frequency value at $t=0$ and f the frequency value at t.

$$\Delta f = \Delta f_0 * e^{-k_{diss}*(t-t_0)} \quad (1b)$$

The k_{diss}/k_{ass} ratio yields the kinetic equilibrium constant k_D (Eq. 1c).

$$k_D = \frac{k_{diss}}{k_{ass}} \quad (1c)$$

2.5. CV-experiments

CV experiments were performed with a CHI-430 computerized, time-resolved electrochemical QCM (CH Instruments Inc., Austin, TX, USA). The working electrode is displayed by the gold coated quartz crystal (diameter 13.7 mm, electrode diameter 5 mm). An Ag/AgCl electrode filled with 3 M aqueous KCl and a platinum wire were used as reference electrode and counter electrode, respectively. The quartz crystal was inserted at the bottom of a Teflon® cell (3 ml cell volume). 5 mM $K_3[Fe(CN)_6]$ was soluted in 0.1 M Na_2SO_4 (background electrolyte) and used as redox-active substance. Potentials ranging from −0.05 to 0.6 V were applied to the working electrode with a scan rate of 10 mV s^{-1}. Substance solutions were added approximately after 35 scans; overall 70 scans were recorded for each experiment.

All experiments were performed at 25 °C. 300 µM stock solutions were diluted to final concentrations of 1.5 µM and 15 nM, respectively, related to the volume of the measurement cells.

2.6. AFM measurements

The lipid films were prepared as described above and investigated immediately after preparation. AFM images were obtained on a Nanowizard® (JPK instruments, Berlin, Germany) and on a Digital Nanoscope IV Bioscope (Veeco Instruments, Santa Barbara, CA). The microscopes were vibration-damped. Commercial pyramidal Si_3N_4 tips (Micromash, Estonia) on a v-shape cantilever with a resonance frequency of about 16 kHz and a nominal force constant of 0.06 N/m were used. All measurements were performed in intermittent contact/Tapping™ mode at a scan speed of approximately 1 Hz to avoid damage of the sample surface. The acquired pictures had a resolution of 512×512 pixels. All measurements were performed in a fluid cell under fully hydrated conditions.

Images were obtained by displaying the amplitude signal of the cantilever in the trace direction, and the height signal in the retrace direction, both signals being simultaneously recorded.

2.7. Laser scanning microscopy and FRAP

For fluorescence microscopy, 1 mol% NBD-PE was inserted as marker into the phospholipid film. The covered glass slides were fixed on an objective slide. Fluorescent images were recorded with a confocal laser scanning microscope (Leica DM IRE2, Leica Microsystems GmbH, Wetzlar, Germany), using a 63×1.4 oil immersion objective at an excitation wavelength of 488 nm and an emission wavelength of 530 nm. In order to detect the fluorescence recovery after photobleaching (FRAP), an area of 53×49 µm was bleached by scanning this area with high intensity laser light within 5 s. The fluorescence recovery was followed by scanning the whole image (81×70 µm) for 25 min (scan frequency: one image per 5 min) and for 5 min (scan frequency: one image per 30 s), respectively.

2.8. Statistical methods

Experiments were repeated for at least three to four times. Data are represented as mean value±standard deviation. The statistical significance of the discussed effects was determined by the unpaired Student's *t*-test. A p value of ≤ 0.05 was considered for statistical significance. Details are described in the figure legends.

3. Results

3.1. QCM-measurements for the detection of peptide membrane bindings

It can be anticipated that the pore formation by nisin depends strongly on the intensity of its membrane binding. In order to focus on this initial step in an isolated and detailed manner, we used QCM as mass sensitive biosensor technique. To simulate the bacterial cell membrane, we covered the quartz surface by support fixed bilayers. In accordance to former studies on the leakage of liposomes by nisin, we applied two different phospholipids for the model membranes, the non-charged DOPC or DOPG, which possesses a net negative charge. In order to consider whether lipid II (Fig. 1) as target for nisin is important for the binding intensity, both membrane types were prepared either in absence or in presence of 0.1 mol% lipid II. Both DOPC and DOPG are fluid lipids forming homogeneous films which tolerate the incorporation of fluid lipid II without any cluster formation. Nisin was applied in two different concentrations which represent the critical amounts for distinction of activity in the presence of lipid II (15 nM nisin) or its absence (1.5 µM nisin). To further evaluate the specificity of binding, we compared nisin with two other peptides (Fig. 1). Reductive methylation of the amino residues of lysine side chains as well as of the N-terminus leads to the formation of methylated nisin. It also possesses a fourfold net positive charge but a reduced binding capacity compared to unmodified nisin, and it is unable to form pores [30].

Insulin was chosen as non-functional blank to evaluate the influence of an overall net positive charge on the peptide membrane effects. Since the B-chain of the insulin does not

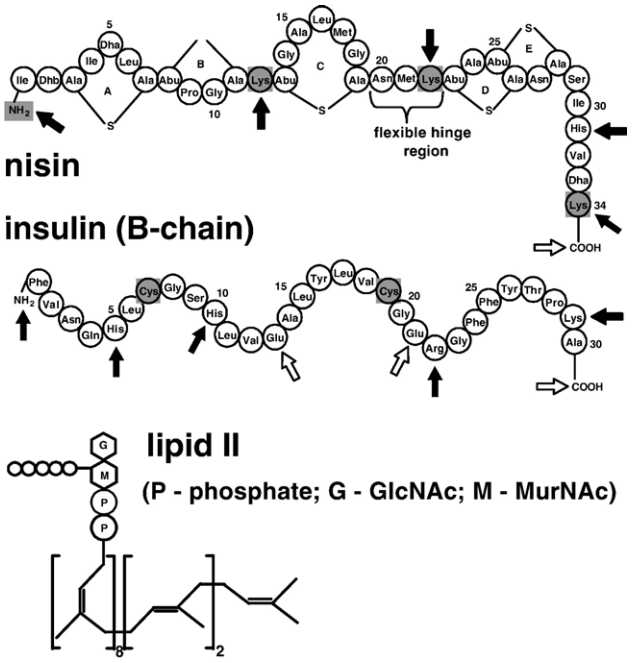

Fig. 1. Amino acid sequence of nisin and insulin. Nisin consists of 34 amino acids (MW 3330 Da), altogether forming five lanthionine rings (A–E), and a flexible hinge region. The molecule has a fourfold net positive charge. Methylation results in eight additional methyl groups (two at each lysine residue and two at the N terminus, as indicated by grey circles) without loss of the net positive charge. The oxidized B chain of insulin consists of 30 amino acids. The molecule has a comparable molecular weight to nisin (3496 Da) and a twofold net positive charge. The two cystein residues (grey circles) are sulfated. Negatively charged amino acid residues of the peptides are marked by open arrows, positively charged by filled ones. The bacterial target lipid II displays two N-acetylated sugars (MurNAc and GlcNAc) linked via pyrophosphate to an undecaprenyl tail. Five amino acid residues (white circles) are linked to MurNAc.

have any intramolecular ring structures or bridging patterns, no specific interaction between the peptide and lipid II will be expected and all effects will be related to unspecific nature.

The QCM measurements were performed in a flow chamber. After equilibrating the resonance frequency of the membrane covered quartz under flow conditions, the addition of the indicated peptide into the medium and subsequent binding onto the membrane can be followed in real time, as illustrated in Fig. 2A. The drop in frequency (black) correlates with the binding of 15 nM peptide. Binding process is completed within 3 min. This time range was independent on the peptide amount and identical, when hundred or thousand fold higher concentrations were used (data not shown).

Kinetic binding constants which should most sensitively illustrate binding characteristics were calculated from the frequency slopes and summarized in Table 1. Considering nisin, the binding onto neutral DOPC membranes is strongly influenced by lipid II which increases the association rate by factor 6. This results in a nearly fourfold higher binding rate. The value for the DOPC/lipid II system (k_D 2.68×10^{-7} M) correspond to the recently published binding constant of 2×10^{-7} M for nisin [11]. Lipid II does not influence the dissociation of the peptide.

Due to charge interactions, nisin binds stronger onto the negatively charged DOPG than onto DOPC (k_D of 3.13×10^{-7} vs. 1.03×10^{-6} M) which is also stronger than recently described [33]. The increase in nisin binding to DOPG by lipid II is only marginal (k_D of 3.13×10^{-7} M vs. 2.11×10^{-7}M). However, the identical k_D for nisin binding to DOPC and

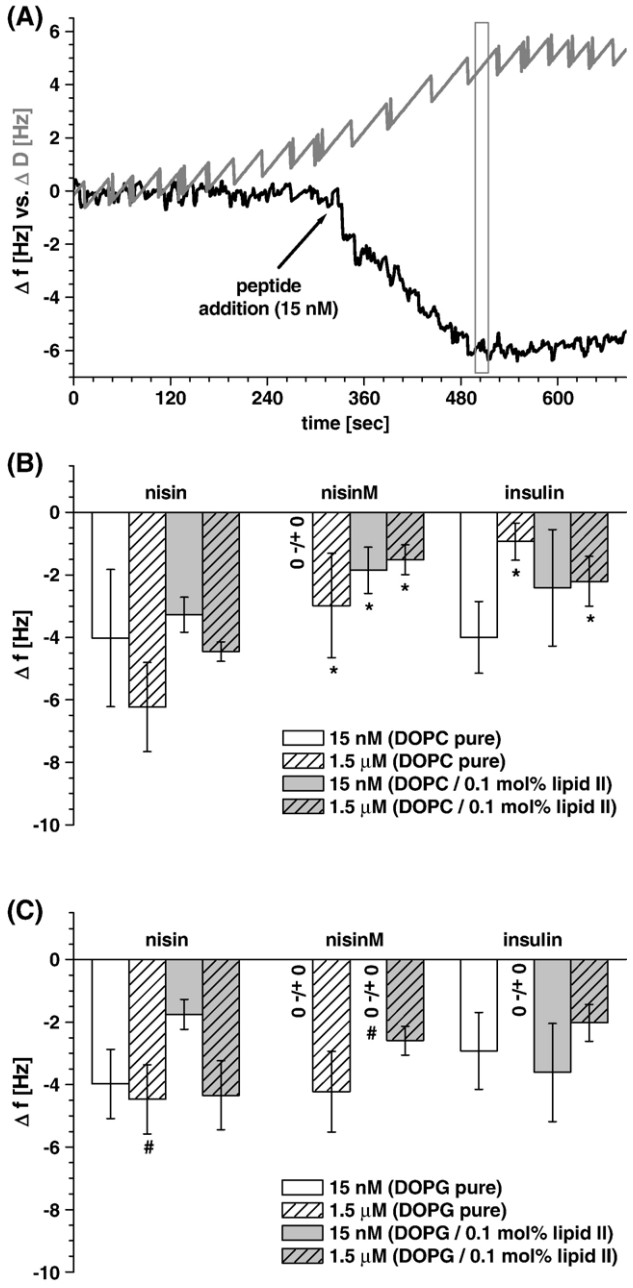

Fig. 2. QCM investigations of the peptide binding. (A) After equilibrating the resonance frequency of the membrane covered quartz crystal, the peptide binding can be followed in real time by detecting the frequency (black line) and damping (grey line) changes. A frequency minimum (corresponding to a binding maximum) is reached within 3 min (marked by a crossbar). (B) displays peptide binding to uncharged DOPC and (C) to negative charged DOPG membranes. No distinct differences in nisin binding could be detected between DOPC and DOPG. The presence of lipid II does not induce an increased peptide binding. Insulin binds similar to nisin, whereas methylated nisin shows a slightly reduced binding. Statistical significance at $p \leq 0.05$ is marked with * for methylated nisin (nisinM) and insulin compared to the corresponding nisin value, with # for DOPG data compared to DOPC values, and with ▪ for the membrane containing lipid II compared to them without the docking molecule.

Table 1
Kinetic constants of nisin binding to DOPC or DOPG membranes in absence or presence of 0.1 mol% lipid II compared to nisinM and insulin as control

		k_{ass} (M^{-1}* s^{-1})	k_{diss} (s^{-1})	k_D (M)
Nisin	DOPC	751.96±105.84	$7.7\times10^{-4}\pm4.16\times10^{-5}$	$1.03\times10^{-6}\pm1.16\times10^{-7}$
	DOPC/0.1 mol% lipid II	4676.58±307.47▪	$1.77\times10^{-3}\pm2.95\times10^{-4}$▪	$2.68\times10^{-7}\pm1.74\times10^{-7}$▪
	DOPG	652.8±119.94	$2\times10^{-4}\pm7.5\times10^{-5}$	$3.13\times10^{-7}\pm1.34\times10^{-7}$#
	DOPG/0.1 mol% lipid II	643.83±255.64#	$1.58\times10^{-4}\pm9.43\times10^{-5}$#	$2.11\times10^{-7}\pm9.93\times10^{-8}$
nisinM	DOPC	2257.94±1001.81*	$2.44\times10^{-3}\pm5.26\times10^{-4}$*	$1.42\times10^{-6}\pm4.26\times10^{-7}$
	DOPC/0.1 mol% lipid II	2430.05±271.85*	$1.58\times10^{-3}\pm6.43\times10^{-4}$	$7.17\times10^{-7}\pm1.96\times10^{-7}$*,▪
	DOPG	1137.45±582.95*	$3.26\times10^{-3}\pm1.53\times10^{-3}$	$1.76\times10^{-6}\pm5.14\times10^{-7}$*
	DOPG/0.1 mol% lipid II	1708.10±706.82*	$1.43\times10^{-4}\pm9.02\times10^{-5}$#,▪	$1.38\times10^{-7}\pm7.29\times10^{-8}$#,▪
Insulin	DOPC	535.92±246.57	$6.33\times10^{-4}\pm2.99\times10^{-4}$	$1.62\times10^{-6}\pm1.5\times10^{-6}$
	DOPC/0.1 mol% lipid II	2431.21±1350.04*	$1.81\times10^{-3}\pm2.84\times10^{-4}$▪	$1.34\times10^{-6}\pm5.98\times10^{-7}$*
	DOPG	1440.67±329.6*,#	$1.99\times10^{-3}\pm1.11\times10^{-3}$*	$2.59\times10^{-6}\pm1.76\times10^{-6}$
	DOPG/0.1 mol% lipid II	2118.65±264.32*▪	$1.27\times10^{-3}\pm6.01\times10^{-4}$*	$6.19\times10^{-7}\pm2.98\times10^{-7}$

The presence of lipid II strongly increases the binding affinity and the association rate of nisin to DOPC membranes. Due to a charge-induced membrane attraction of nisin to DOPG, the effect of lipid II for increasing the association rate is less pronounced. Methylated nisin displays lower binding affinity compared to nisin, the binding of insulin is not influenced by the presence of lipid II, indicating an unspecific nature of protein membrane interactions.
Statistical significance at $p \le 0.05$ is marked with * for methylated nisin and insulin compared to the corresponding nisin value, and with # for DOPG data compared to DOPC values, and with ▪ for comparing membranes containing lipid II to membranes without lipid II.

DOPG in presence of lipid II (k_D 2.68×10^{-7}M vs. 2.11×10^{-7}M) emphasize the role of lipid II for binding. The fact that lipid II overlays a charge impact in nisin binding has also been postulated by others [11].

The absolute frequency changes representing the total bound masses are summarized in Fig. 2B and C. Despite the evident effects of lipid II on binding kinetics, an increase in total amount of nisin bound was not evident in presence of lipid II. Furthermore, we could not detect distinct differences between DOPC (Fig. 2B) and DOPG (Fig. 2C) membranes; although a stronger binding to DOPG could be anticipated, as observed by others [34]. On both membranes the higher nisin concentration only displayed a marginal stronger binding.

The methylation of nisin diminishes the binding ability compared to nisin which is reflected by both, the kinetic data in Table 1 as well as the frequency drops in Fig. 2. The effect of lipid II on binding kinetics is less distinct, only the binding onto DOPG/lipid II membranes is identical to nisin. Again, an effect of lipid II on bound protein mass is not evident.

As expected, insulin as blank peptide displays a lower binding activity in general. Neither the kinetic constants nor the absolute frequency shifts correlate with an effect of lipid II and do not allow interpreting specific binding factors. Charge-induced interactions appear responsible for the higher binding onto DOPG than DOPC (Fig. 2), but the stronger binding of the lower concentration cannot be explained.

To characterize the mode of peptide membrane binding, we analyzed the damping frequency which is illustrated in Fig. 2A as a grey line. The damping frequency correlates with the viscoelastic properties of the sensor bound analytes and therefore allows further binding interpretations. We detected the changes in damping frequency within the indicated time range. For a proper evaluation we related these data to the resonance frequency changes. *D*/*f* slopes represent time-independent absolute data (Table 2) and reflect the viscoelasticity on the membrane surface. In absence of lipid II, the data of methylated nisin and insulin are lower for DOPG than for DOPC. This indicates a tighter binding of the positively charged peptides to the negatively charged membrane than to the neutral DOPC. The presence of lipid II changes the *D*/*f* slopes which illustrate that lipid II has an impact on the membrane surface and affects peptide attachment.

However, the nisin data behave significantly different and display a much higher value in case of the pure DOPG com-

Table 2
Slopes of *D*/*f* plots reflect viscoelasticity of the membrane

	pure DOPC	DOPC & 0.1 Mol% lipid II	pure DOPG	DOPG & 0.1 Mol% lipid II
15 nM nisin	| 0.732±0.213 |	| −0.783±0.167 |	| −1.033± 0.367 |	| −1.635±0.24 |#
1.5 μM nisin	| 0.594±0.214 |	| −1.494±0.36 |▪	| −2.902±1.501 |	| −1.043±0.295 |
15 nM nisin*	| −0.528±0.045 |	| 0.146±0.066 |*▪	| −0.302±0.029 |*#	| −0.64±0.342 |*
1.5 μM nisin*	| −1.606±0.389 |*	| 0.301±0.149 |*▪	| −0.331±0.193 |*	| 0.855±0.387 |#
15 nM insulin	| −0.673±0.3 |	| −0.660±0.240 |	| −0.335±0.155 |*	| −0.592±0.388 |*
1.5 μM insulin	| −0.751±0.077 |	| −0.986±0.626 |	| −0.613±0.144 |	| −0.63±0.28 |

Plotting the damping (*D*) against the frequency (*f*) values represents time-independent information on membrane surface characteristics. In absence of lipid II the DOPG data of methylated nisin and insulin (highlighted in light grey) are lower compared to DOPC indicating a tighter binding of the positive peptides to the negative membrane. The nisin data (highlighted in dark grey) display much higher values for pure DOPG compared to pure DOPC. This indicates a highly viscous surface structure, hypothetically related to the formation of vesicular structures on the surface. The presence of lipid II in DOPG membranes results in lower *D*/*f* slopes showing a membrane stabilizing effect of lipid II. Statistical significance at $p \le 0.05$ is marked with * for methylated nisin and insulin compared to the corresponding nisin value, and with # for DOPG data compared to DOPC values, and with ▪ for comparing membranes containing lipid II to membranes without lipid II.

pared to the pure DOPC membrane. This indicates a highly viscous surface structure which is typically induced by molecular associations. It would correspond with former findings that positively charged peptides, when contacting negatively charged membranes, are able to extract lipids out of the membrane assembly and generate micellar or vesicular associates. This effect has been described as "carpet mechanism" by Shai [35] and was also observed for pardaxin on POPC membranes [36].

AFM images (Fig. 3) strongly support this hypothesis. Whereas the pure DOPG film (Fig. 3A) displays a plain surface, nisin induces the formation of round vesicular structures in the 100 nm range (Fig. 3B). Lipid II (0.1 mol%) appears to be homogeneously distributed in the DOPG membrane, giving no indication for phase separations (Fig. 3C). In presence of lipid II, the addition of nisin does not induce the formation of the surface vesicles (Fig. 3D) as observed in the pure DOPG membranes. The image indicates a homogenous (lower part) and particularly strong and clustered adhesion of the peptide (upper part), which cannot fully be elucidated.

The fact that the structure of the pure DOPC film (Fig. 3E) is not affected by nisin (Fig. 3F) emphasizes the impact of charge-induced protein interaction.

3.2. CV investigations to follow nisin induced pore formation

In order to investigate changes in membrane permeability by pore formation, we applied CV measurements. In former studies we optimized the CV measurements in respect to bilayer permeability detection [32]. We could show that the membrane forming steps on the quartz surface, beginning with an immobilized monolayer and followed by bilayer completion, lead to a dramatic insulation against electrode transfer. This strongly flattens the Faradaic current (Fig. 4A) which complicates a common evaluation including the peak currents and the distance between the peaks. Therefore, changes in membrane permeability were analyzed by integrating the area between two single scans, resulting in a time-resolved illustration of the electrical charge (Fig. 4B). A detailed charge calculation from CV curves was previously described [32]. The changes of the Faradaic current after peptide addition, calculated from the time resolved illustration of the electrical charge, were presented as histograms (Fig. 5).

Considering the effects in a DOPC membrane (Fig. 5A), the data strongly confirm a nisin-induced pore formation and the essential role of lipid II. Whereas in absence of lipid II, both concentrations of nisin display only a marginal membrane permeabilization, the presence of lipid II increases the effects by the factor 2 (15 nM nisin) and 5 (1.5 μM nisin), respectively. This is fully corresponding to earlier findings. Nanomolar concentrations of nisin are sufficient for pore formation when lipid II acts as a target molecule [37]. Insulin as control displays certain effects on membrane permeability which could neither be explained nor correlated to peptide concentration and lipid II presence. The small amount of methylated nisin (15 nM) does not show any current increase, but a hundredfold higher concentration causes a distinct current increase which could partly be related to unspecific membrane damages.

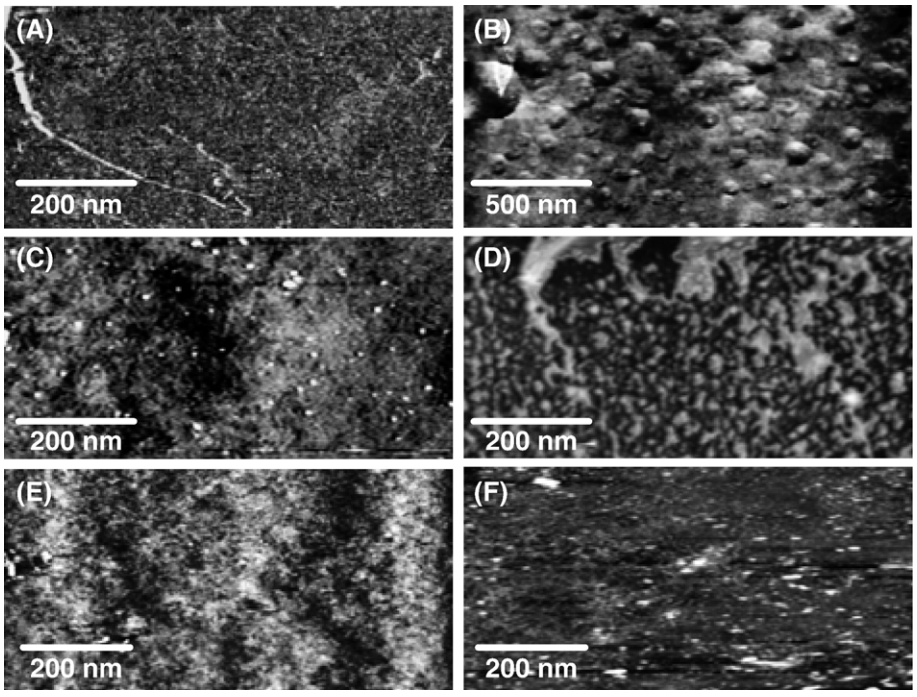

Fig. 3. AFM images of the model membrane used. Whereas the pure DOPG film (A) appears as even membrane surface, the addition of 1.5 μM Nisin induces the formation of round vesicular structures in the 100 nm range (B). The DOPG/lipid II (99.9/0.1) membrane (C) gives no indication for lateral separation of lipid II. The interaction of 1.5 mM nisin with the DOPG/lipid II membrane (D) is manifested in a surface attachment of small, and partly agglomerated structures, but the membrane peculiarities illustrated in (B) are not evident. The pure DOPC membrane (E) is not disturbed by 1.5 μM Nisin (F) in contrast to DOPG (B). Any pore formation by nisin is not evidently illustrated.

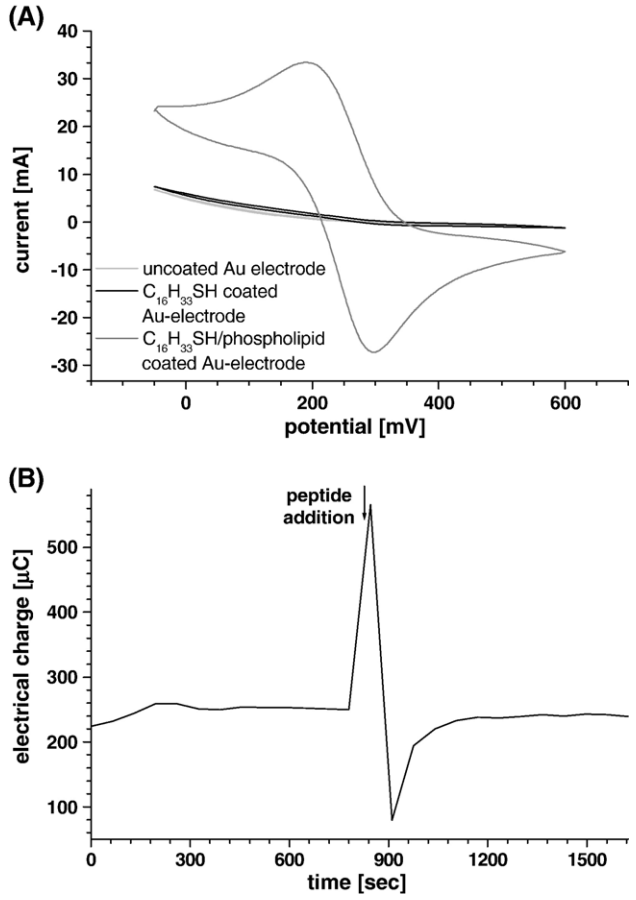

Fig. 4. CV measurements to detect permeability changes. (A) The immobilization of a hexadecanethiol monolayer on the gold electrode inherently flattens the Faradaic current. The current is further decreased by additional coating with phospholipids resulting in a bilayer. (B) Since a common evaluation including peak currents and peak distance is not available, the area between two single scans is integrated, resulting in a time resolved illustration of the electrical charge.

The effects of nisin on the charged DOPG membrane (Fig. 5B) are principally the same than on DOPC. However, even though the proportion is identical, all preparations lead to a higher permeability of the charged membrane. Again, the importance of lipid II becomes evident since the nanomolar nisin concentration induces a nearly 100% current increase, strongly exceeding the effect of the micromolar nisin in absence of lipid II. Without any doubts, charge-induced interactions between peptide and membrane are partly responsible for the higher level of effects. However, the low and the high nisin amount display similar effects in absence of lipid II, although much higher data would be anticipated for the millimolar concentration, referring to the postulated unspecific membrane damage from the *D*/*f* plots in Table 2.

The impact of charge-induced interactions can also explain the insulin data, since the positively charged control peptide causes a certain membrane permeabilization, regardless of lipid II.

In DOPG membranes, methylated nisin displays a current increase of about 50% only in absence of lipid II. The lower *D*/*f* slopes, compared to nisin, imply that the generation of molecular associates might not be responsible for the permeability increase. Probably, methylated nisin causes a contraction of DOPG molecules, leading to a tighter arrange-

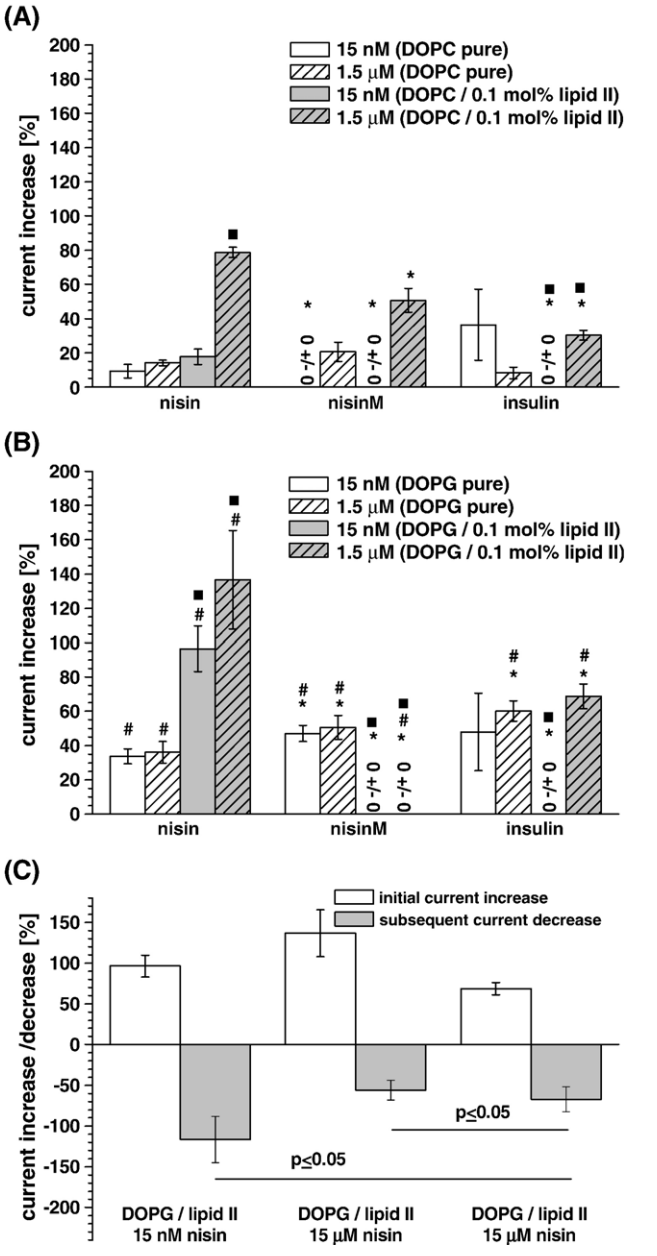

Fig. 5. CV investigations to illustrate nisin induced pore formation and the role of lipid II. (A) While nisin only shows an unspecific small current increase on pure DOPC membranes, the presence of lipid II raises the current by factor 2 (15 nM nisin) and 5 (1.5 µM nisin). A certain membrane permeabilization by methylated nisin was only observed at 1.5 µM concentrations. (B) The nisin effects on the negatively charged DOPG membranes are stronger pronounced. Both, nisin and methylated nisin, show an unspecific current increase by interacting with lipid II free DOPG membranes, indicating a membrane structure disorder. Pore formation was not observed for methylated nisin. (C) The initial current increase of DOPG/lipid II membranes was followed by a current decrease; a further charge induced peptide attachment and insulation of the electrode is assumed. Statistical significance at $p \leq 0.05$ is marked with * for methylated nisin and insulin compared to the corresponding nisin value, with # for DOPG data compared to DOPC values, and with ▪ for comparing membranes containing lipid II to membranes without lipid II.

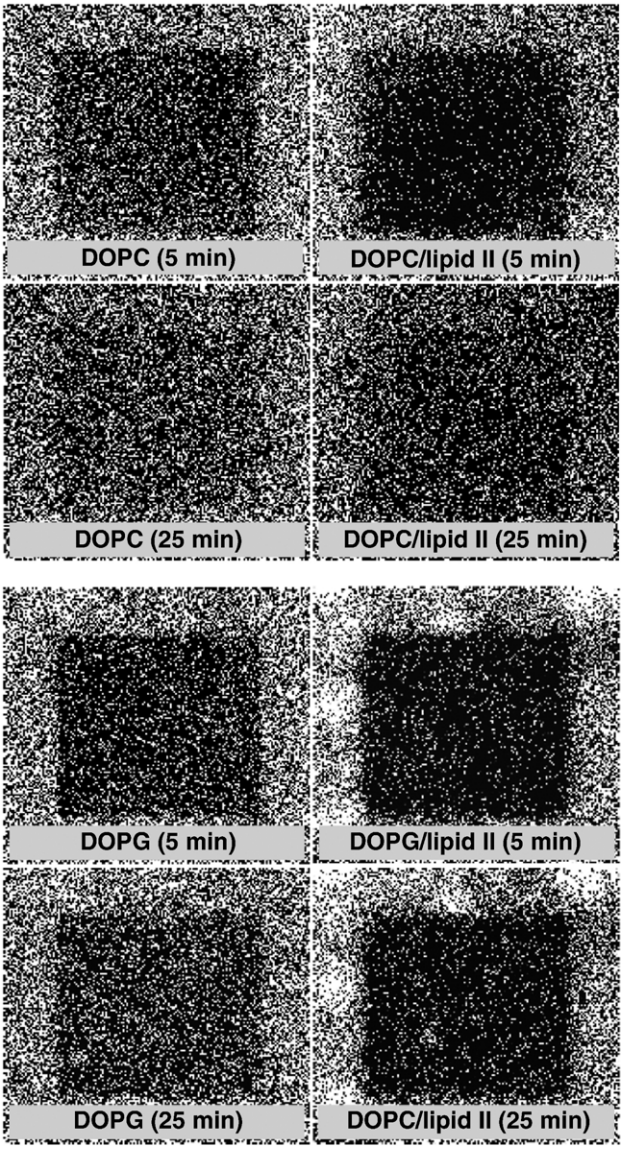

Fig. 6. Fluorescence recovery after photobleaching (FRAP) experiments to illustrate the lateral diffusion and the membrane stabilizing effect of lipid II. In one area of each film the fluorescence was quenched, resulting in a complete black domain (not shown). The slides illustrate the reappearance of fluorescence in the bleached domains as indicator for diffusion of lipids, e.g. fluorescence markers. Fluorescence intensity was recorded every 5 min—the pictures show fluorescence levels 5 and 25 min after bleaching. A reduced lateral diffusion (lower fluorescence intensity in the bleached area) was detected in the lipid II containing DOPC and DOPG films compared to the pure phospholipids. This correlates with a stabilizing effect of lipid II on the lateral membrane constitution.

ment of the peptides at the membrane. The postulated membrane stabilizing effect of lipid II inhibits this contraction and subsequently a current increase.

The assumption that charge-induced interactions of the peptides with the DOPG membrane influence the data is supported by the findings presented in Fig. 5C. Only in case of the DOPG/lipid II membrane, the permeability decreases dramatically below the starting level after the initial permeabilization. This should be attributed to a further charge induced peptide attachment to the membrane surface which insulates the membrane after the specific pore formation. The peptide amount for this secondary effect appears to be small since the QCM courses (Fig. 2B and C) did not give any indications for massive bindings. This correlates with the finding that the permeability decrease is independent of the peptide amount.

Since the drop in permeability could only be observed in presence of lipid II, this leads to further interpretation of a stabilizing role of lipid II for the model membranes.

3.3. Fluorescence microscopic investigation of lipid II membrane effects

Besides its role as a target for nisin and pore constituent, a further function of lipid II in model membranes can be assumed. Since the size of the hydrophobic moiety of lipid II exceeds the thickness of a monolayer, the insertion of lipid II in a membrane will increase the contact of both monolayers, partly reducing the ability for vertical diffusion of the matrix lipids. This should not contradict the role of lipid II as pore constituent in a fluid membrane. Whether the postulated anchoring by lipid II decreases the lateral membrane diffusion was evaluated by fluorescence recovery after photobleaching. The bleaching of a lipid-bound fluorescence marker within a certain area of a model membrane is the basis to microscopically evaluate the time dependency for diffusion of marker molecules into the bleached area.

In analogy to the quartz sensors, DOPC and DOPG model membranes with and without 0.1 mol% lipid II were prepared. They contained 1 mol% of the fluorescence dye NBD-PE and were transferred to microscopic slides. With the help of a laser scanning microscope, an area of about 53 × 49 mm was bleached. The diffusion of fluorescence into this area was followed by a sequence of microscopic images, as illustrated in Fig. 6.

It is evident that despite individual differences, lipid II reduces the lateral diffusion of both lipids which corresponds our postulation. It was not the intention to calculate the exact lateral diffusion velocity. But to support this optical evidence, we analyzed the pixel intensity of the bleached area in time dependency for 25 min. To avoid dysfunctions due to the general bleaching of the membranes, we sensitively analyzed the slope within the first 5 min at a scan sequence of 30 s, as illustrated in Table 3.

These data confirm that the presence of lipid II reduces the lateral diffusion of DOPC to about 50%. DOPG itself has a much lower lateral diffusion ability compared to DOPC in this

Table 3
Confirmation of the membrane stabilizing effect of lipid II

	Pure phospholipid film	Phospholipid film and 0.1 mol% Lipid II
DOPC	$2.62\times10^{-2}\pm1.94\times10^{-2}$	$1.49\times10^{-2}\pm7.78\times10^{-5}$
DOPG	$5.03\times10^{-3}\pm3.68\times10^{-4}$	1.35×10^{-3}

In further FRAP experiments the fluorescence intensity was measured every 30 s within 5 min after bleaching; the slope of the fluorescence intensity/time curve was calculated and is illustrated here. The presence of lipid II in DOPC and DOPG reduces the lateral diffusion of membrane lipids by about 50% and 25%, respectively.

study. However, the influence of lipid II is even much stronger and diminishes the diffusion rate to about 25%. The appearance of fluorescent spots in the DOPG/lipid II membrane should be a matter of further evaluations.

4. Discussion

In this study we applied two combined biosensors to analyze the molecular events of nisin leading to cell death with respect to nisin membrane interaction, pore formation, and the role of lipid II. Several studies have already been performed referring to the pore formation of nisin using different model membrane systems. In most cases, the marker release from liposomes by nisin was used to define the molecular mechanisms of pore formation and the essential role of lipid II [11,34,38]. Recent data confirm that lipid II is recruited by nisin as a constituent of the pores which are of constant structure and nisin–lipid II stoichiometry [12–14,37].

Our biosensor approach gives further insight into these mechanisms. QCM as mass sensitive sensor was combined with CV to correlate the binding of nisin onto a planar model membrane with pore forming in real time. Both techniques were referred to the role of lipid II, the nisin concentration and membrane characteristics.

The QCM assay allows for the first time to solely focus on the nisin binding characteristics by analyzing both, the binding kinetics as well as the absolute amount of bound nisin. Lipid II as a target for nisin has an essential role in the initial binding phase which is evident by a sixfold higher association rate of nisin onto DOPC membranes containing 0.1 mol% lipid II. This supports the role of lipid II in an early phase of nisin contact to the bacterial membrane. Although nisin binds stronger to the plain DOPG membrane than on plain DOPC due to charge effects, lipid II overcomes these differences resulting in identical binding constants for both systems. Following the binding process for several minutes, these initial differences in binding affinity do not influence the absolute amount of bound nisin. The frequency changes in Fig. 2 demonstrate no stronger binding of nisin in presence of lipid II. Furthermore, we could not find a correlation of bound nisin with nisin concentrations, since hundredfold higher amounts show only slightly stronger binding. This might indicate that the amount of nisin binding is not limiting the activity.

To evaluate the amount of bound nisin, the detected frequency changes were calculated according to the Sauerbrey equation (Eq. 2), where Δf is the frequency change, f_0 the fundamental resonance frequency, A the area of the quartz crystal, ñ the density, μ the shear modulus of the quartz crystal, and Δm the mass change [18]:

$$\Delta f = -\frac{2f_0^2}{A\sqrt{\mu_q \rho_q}}\Delta m = -C_f \Delta m \quad (2)$$

Regarding the sensitive surface of the quartz sensor, a frequency change by 1 Hz corresponds to a mass increase of 1.24 ng. The frequency changes in Fig. 2B correspond to a binding of about 1.22 to 2.3 pmol nisin.

Since we could not detect an influence by the presence of lipid II, a correlation of the nisin amount with the number of lipid II molecules appears useful. The sensitive area of the sensor is covered by about 7×10^{13} phospholipid molecules, referring to a mean head size of about 40 Å^2. Consequently, 0.1 mol% lipid II would roughly correspond to 7×10^{10} molecules, respectively 0.7 pmol. This correlates with a molar ratio of nisin/lipid II ratio of 2:1 at the nanomolar concentration, or 3:1 at the micromolar nisin amount. However, the binding ratio of 2:1 for the nanomolar concentration excellently corresponds with previous findings on the constant pore stoichiometry of nisin/lipid II in a ratio of 2:1 [14]. These findings help to explain the mechanism of nisin activity. 15 nM nisin binds to the membrane surface with an affinity increasing effect of lipid II. The nanomolar concentration fits perfectly with 0.1 mol% lipid II to induce the pore formation. Hasper et al. reported that nisin recruits all available lipid II for pore formation [14]. This can also be a reason that hundredfold higher nisin amounts do not possess clearly increased membrane permeabilization, as illustrated by the CV data of DOPG (Fig. 5B).

Considering the control peptides, the methylation of nisin does not only impair the pore forming properties, it also reduces the binding affinity (Table 2) and binding intensity (Fig. 2). An effect of lipid II is less pronounced as for nisin. Insulin as blank peptide displays lower bindings, independent of lipid II.

The CV experiments prove the essential function of lipid II for pore formation (Fig. 5). The CV data allow an evaluation of the long term pore stability. Whereas the increase in the Faradaic current, respectively the pore formation, occurres within a single scan of about 65 s, the current remains stable within the total time of detection of 35 min. The observed pore stability again corresponds with the results described by Hasper et al. [14].

The DOPG lipid II membranes give further causes for interpretation. In this system, the initial current increase was followed by a drop in current below the base line. This might indicate that independent on the obvious stability of the pores, further peptide molecules attach charge-induced to the membrane and unspecifically occlude the pores. Nisin behaves similar to the insulin control peptide which emphasizes the role of charge. The neutral DOPC membranes do not show this phenomenon. However, the attached amounts of peptide appear to be low, since they are not detectable in the QCM frequency course. Furthermore, this process occurs only in presence of lipid II which indicate a potential membrane stabilizing function of lipid II. A stabilizing effect has also been proven by measuring the *D*/*f*-slopes of DOPC and DOPG membranes without peptide addition. The presence of 0.1 mol% lipid II decreased the *D*/*f*-slope in both phospholipids, indicating a more rigid and stabilized film. In principle identical, but stronger pronounced effects were detected when replacing lipid II by 0.1 mol% of cholesterol as established membrane stabilizer. The *D*/*f*-slope of pure DOPC (0.518) was reduced by lipid II and cholesterol (0.456 vs. 0.300), and of pure DOPG (0.574) to 0.465 and 0.270, respectively.

In absence of lipid II, the DOPG membrane is disturbed by high nisin concentrations. We postulated a carpet-like extraction

of negative lipids out of the membrane by positive peptides [35] from the damping slope in Table 2. This hypothesis and the value of damping analysis could be strongly confirmed by AFM images which illustrate loosely attached vesicles formation. In contrast, lipid II seems to anchor the membrane network. The structure of the hydrophobic moiety of lipid II should allow a dynamic contact of both membrane leaflets. This will not lead to a static conservation of the lateral membrane structure which would contradict the pore formation, but the lateral membrane diffusion should be reduced by lipid II. The FRAP data confirm this postulation and clearly illustrate a strong reduction in lateral diffusion in membranes with lipid II.

Summarizing, both biosensor techniques give further insights into nisin antibiotic activity and the role of lipid II in this model membrane system. Lipid II possesses an essential affinity increase for nisin binding, but it does not directly influence the amount of peptide binding. The peptide amount is no limit for the pore formation. Whereas earlier studies postulated that high nisin concentrations create pores in absence of lipid II, we illustrate other types of unspecific membrane damages. In that context, a physical stabilizing effect of lipid II became evident by microscopic images.

Acknowledgements

We thank M. Josten (University of Bonn) for mass determination of the peptides, U. Rothe (University of Halle) for assistance in FRAP experiments, H.-H. Rüttinger (University of Halle) for discussing the electrochemical data and the German Research Foundation (DFG) for financial support (GRK 677 and Sa 292/9-4).

References

[1] A.T.R. Mattick, A. Hirsch, A powerful inhibitory substance produced by group N streptococci, Nature 154 (1944) 551.
[2] A. Hurst, Nisin, Adv. Appl. Microbiol. 27 (1981) 85–123.
[3] E. Gross, J.L. Morell, The structure of nisin, J. Am. Chem. Soc. 93 (1971) 4634–4635.
[4] H.-G. Sahl, G. Bierbaum, Lantibiotics: biosynthesis and biological activities of uniquely modified peptides from gram-positive bacteria, Annu. Rev. Microbiol. 52 (1998) 41–79.
[5] E. Ruhr, H.-G. Sahl, Mode of action of the peptide antibiotic nisin and influence on the membrane potential of whole cells and on cytoplasmic and artificial membrane vesicles, Antimicrob. Agents Chemother. 27 (1985) 841–845.
[6] F. Porcelli, B. Buck, L. Dong-Kuk, K.J. Hallock, A. Ramamoorthy, G. Veglia, Structure and orientation of pardaxin determined by NMR experiments in model membranes, J. Biol. Chem. 279 (2004) 45815–45823.
[7] S.K. Kandasamy, R.G. Larson, Effect of salt on the interactions of antimicrobial peptides with zwitterionic lipid bilayers, BBA 1758 (2006) 1274–1284.
[8] M.P. Boland, F. Separovic, Membrane interactions of antimicrobial peptides from Australian tree frogs, BBA 1758 (2006) 1178–1183.
[9] R. Volinsky, S. Kolusheva, A. Berman, R. Jelinek, Investigations of antimicrobial peptides in planar film systems, BBA 1758 (2006) 1393–1407.
[10] K. Nomura, G. Corzo, The effect of binding of spider-derived antimicrobial peptides, oxyopinins, on lipid membranes, BBA 1758 (2006) 1475–1482.
[11] I. Wiedemann, E. Breukink, C. van Kraaij, O.P. Kuipers, G. Bierbaum, B. de Kruijff, H.-G. Sahl, Specific binding of nisin to the peptidoglycan precursor lipid II combines pore formation and inhibition of cell wall biosynthesis for potent antibiotic activity, J. Biol. Chem. 276 (2001) 1772–1779.
[12] I. Wiedemann, R. Benz, H.-G. Sahl, Lipid II-mediated pore formation by the peptide antibiotic nisin: a black lipid membrane study, J. Bacteriol. 186 (2004) 3259–3261.
[13] E. Breukink, H.E. van Heusden, P.J. Vollmerhaus, E. Swiezewska, L. Brunner, S. Walker, A.J.R. Heck, B. de Kruijff, Lipid II is an intrinsic component of the pore induced by nisin in bacterial membranes, J. Biol. Chem. 278 (2003) 19898–19903.
[14] H.E. Hasper, B. de Kruijff, E. Breukink, Assembly and stability of nisin–lipid II pores, Biochemistry 43 (2004) 11567–11575.
[15] S.T. Hsu, E. Breukink, E. Tischenko, M.A. Lutters, B. de Kruijff, R. Kaptein, A.M. Bonvin, N.A. van Nuland, The nisin–lipid II complex reveals a pyrophosphate cage that provides a blueprint for novel antibiotics, Nat. Struct. Mol. Biol. 11 (2004) 963–967.
[16] T. Vo-Dinh, B. Cullum, Biosensors and biochips: advances in biological and medical diagnostics, Fresenius J. Anal. Chem. 366 (2000) 540–551.
[17] D.R. Thévenot, K. Toth, R.A. Dust, G.S. Wilson, Electrochemical biosensors: recommend definitions and classification, Biosens. Bioelectron. 16 (2001) 121–131.
[18] G. Sauerbrey, Verwendung von Schwingquarzen zur Wägung dünner Schichten und zur Mikrowägung, Z. Phys. 155 (1959) 206–222.
[19] H. Xu, J.B. Schlenoff, Kinetics, isotherms, and competition in polymer adsorption using the quartz crystal microbalance, Langmuir 10 (1994) 241–245.
[20] S. Kurosawa, H. Aizawa, J. Miyake, M. Yoshimoto, J. Hilborn, Z.A. Talib, Detection of deposition rate of plasma-polymerized silicon-containing films by quartz crystal microbalance, Thin Solid Films 407 (2002) 1–6.
[21] Y. Hoshino, T. Kawasaki, Y. Okahata, Effect of ultrasound on DNA polymerase reactions: monitoring on a 27-MHz quartz crystal microbalance, Biomacromolecules 7 (2006) 682–685.
[22] G.S. Huang, M.T. Wang, M.Y. Hong, A versatile QCM matrix system for online and high-throughput bio-sensing, Analyst 131 (2006) 382–387.
[23] K. Glasmastar, C. Larsson, F. Hook, B. Kasemo, Protein adsorption on supported phospholipid bilayers, J. Colloid. Interface Sci. 246 (2002) 40–47.
[24] C. Zhou, J.M. Freidt, A. Angelova, K.H. Choi, W. Laureyn, F. Frederix, L.A. Francis, Y. Campitelli, G. Engelborghs, Human immunoglobulin adsorption investigated by means of quartz crystal microbalance dissipation, atomic force microscopy, surface acoustic wave, and surface plasmon resonance techniques, Langmuir 20 (2004) 5870–5878.
[25] A.S. Viana, L.M. Abrantes, G. Jin, S. Floate, R.J. Nichols, M. Kalaji, Electrochemical, spectroscopic and SPM evidence for the controlled formation of self-assembled monolayers and organised multilayers of ferrocenyl alkyl thiols on Au (111), Phys. Chem. Chem. Phys. 3 (2001) 3411–3419.
[26] R. Bilewicz, Bifunctional monomolecular Langmuir–Blodgett films at electrodes, electrochemistry at single molecule “Gate Sites”, J. Am. Chem. Soc. 113 (1991) 5464–5466.
[27] O.P. Kuipers, H.S. Rollema, W.M. Yap, H.J. Boot, R.J. Siezen, W.M. de Vos, Engineering dehydrated amino acid residues in the antimicrobial peptide nisin, J. Biol. Chem. 267 (1992) 24340–24346.
[28] R.R. Bonelli, T. Schneider, H.-G. Sahl, I. Wiedemann, Insights into in vivo activities of lantibiotics from gallidermin and epidermin mode-of-action studies, Anitmicrob. Agents Chemother. 50 (2006) 1449–1457.
[29] D. Dottavio-Martin, J.M. Ravel, Radiolabeling of proteins by reductive alkylation with [14C]formaldehyde and sodium cyanoborohydride, Anal. Biochem. 87 (1978) 562–565.
[30] B.B. Bonev, E. Breukink, E. Swiezewska, E.B. de Kruijff, A. Watts, Targeting extracellular pyrophosphates underpins the high selectivity of nisin, FASEB J. 18 (2004) 1862–1869.
[31] T. Schneider, M.M. Senn, B. Berger-Bachi, A. Tossi, H.-G. Sahl, I. Wiedemann, In vitro assembly of a complete, pentaglycine interpeptide bridge containing cell wall precursor (lipid II-Gly5) of *Staphylococcus aureus*, Mol. Microbiol. 53 (2004) 675–685.
[32] K. Christ, H.-H. Rüttinger, M. Höpfner, U. Rothe, G. Bendas, The

detection of UV-induced membrane damages by a combination of two biosensor techniques, Photochem. Photobiol. 81 (2005) 1417–1423.
[33] E. Breukink, P. Ganz, B. de Kruijff, J. Seelig, Binding of nisin Z to bilayer vesicles as determined with isothermal titration calorimetry, Biochemistry 39 (2000) 10247–10254.
[34] E. Breukink, C. van Kraaij, R.A. Demel, R.J. Siezen, O.P. Kuipers, B. de Kruijff, The C-terminal region of nisin is responsible for the initial interaction of nisin with the target membrane, Biochemistry 36 (1997) 6968–6976.
[35] Y. Shai, Mode of action of membrane active antimicrobial peptides, Biopolymers 66 (2002) 236–248.
[36] K.J. Hallock, L. Dong-Kuk, J. Omnaas, H.I. Mosberg, A. Ramamoorthy, Membrane composition determines Pardaxin's mechanism of lipid bilayer disruption, Biophys. J. 83 (2002) 1004–1013.
[37] H.E. van Heusden, B. de Kruijff, E. Breukink, Lipid II induces a transmembrane orientation of the pore-forming peptide lantibiotic nisin, Biochemistry 41 (2002) 12171–12178.
[38] A.J.M. Driessen, H.W. van den Hooven, W. Kuiper, M. van de Kamp, H.-G. Sahl, R.N.H. Konings, W.N. Konings, Mechanistic studies of lantibiotic-induced permeabilization of phospholipid vesicles, Biochemistry 34 (1995) 1606–1614.